An Algebraic Stress Model for Turbulent Mixing Flows Driven by Converging Spherical Shock Waves

Qifan Yang*, Yangjie Shao*, Jin Qi** and Song Fu*
Corresponding author: fs-dem@tsinghua.edu.cn
* School of Aerospace Engineering, Tsinghua University, Beijing 100084, PR China
** Institute of Applied Physics and Computational Mathematics, Beijing 100094, PR China

Abstract: Accurate prediction of Reynolds stress anisotropy remains a key challenge in modeling turbulent mixing driven by converging spherical shock waves. Although many two-equation and BHR-type models can predict the growth of the mixing layer, the linear eddy-viscosity constitutive relations they employ cannot correctly represent the Reynolds stress anisotropy induced by rapid compression, shock-interface interaction, and variable-density effects. This work presents an algebraic stress model that exploits spherical symmetry to obtain a direct closure for the radial Reynolds stress component, thereby avoiding a full Reynolds-stress transport formulation. The closure is incorporated into a modified k–l model and evaluated against high-fidelity ILES data for spherically converging shock-driven mixing. The proposed model maintains the overall accuracy of the baseline approach for bubble/spike evolution and volume fraction profiles, while improving the prediction of Reynolds stress anisotropy in the mixing region. These results suggest that the algebraic stress closure provides an efficient strategy for enhancing anisotropy modeling in compressible variable-density turbulent mixing.

Keywords: Algebraic Stress Model, Turbulent Mixing, Converging Spherical Shock Waves

1. Introduction

Shock-driven turbulent mixing at material interfaces is central to a wide range of high-speed and high-energy-density flows. In inertial confinement fusion, for example, hydrodynamic instabilities and the ensuing turbulent mixing can degrade implosion symmetry, transport cold material into the hot spot, and reduce target performance[1, 2, 3]. Spherically converging shock-driven mixing therefore serves both as a canonical configuration for studying compressible variable-density turbulence and as a simplified model problem for implosion-relevant flows.

For practical simulations of such flows, Reynolds-averaged models remain attractive because of their computational efficiency and compatibility with engineering CFD workflows. Existing variable-density turbulent-mixing closures, including BHR-type models, have been applied with reasonable success in predicting integral quantities such as mixing width and mean profiles[3]. However, many widely used closures rely on isotropic constitutive relation[4] or linear eddy-viscosity assumptions[5] for the Reynolds stress. These approximations are often too simple to represent the flow physics for shock-driven mixing, where the Reynolds stress is strongly anisotropic and closely coupled to pressure gradients, mass flux, and rapid mean-flow distortion. Full Reynolds-stress transport models can, in principle, represent these effects more faithfully, but their additional equations, closure uncertainties, and computational cost limit their use in practical implosion-scale calculations.

These limitations motivate the development of closures that improve Reynolds stress anisotropy predictions while retaining the efficiency of two-equation mixing models. In this work, an algebraic-stress-based turbulent mixing model is developed for spherically converging shock-driven flows. The spherical symmetry of the problem is exploited to derive a compact algebraic relation for the radial Reynolds stress component, avoiding the large tensor-basis expansions commonly used in explicit algebraic stress models. The closure is assessed using high-fidelity Implicit Large Eddy Simulation (ILES) data for a spherically converging Richtmyer–Meshkov instability, where it demonstrates improved representation of Reynolds stress anisotropy.

For practical use, the proposed closure is incorporated into a modified BHR2 framework, leading to a revised $k - l$ formulation. The coupled model is then applied to a spherically converging shock-driven mixing problem and compared with the baseline eddy-viscosity closure. The results show comparable predictions of bubble/spike evolution and volume fraction profiles, together with an improved representation of Reynolds stress anisotropy.

The remainder of this paper is organized as follows. Section 2 introduces the algebraic stress closure and assesses it against ILES data for the spherically converging Richtmyer–Meshkov instability. Section 3 describes the computational framework and the implementation of the turbulence models. Section 4 presents the application to a spherically converging shock-driven mixing problem and compares the results with the baseline eddy-viscosity closure. Conclusions and future directions are given in Section 5.

2. Derivation and Evaluation of the Algebraic Stress Closure

Due to the compressibility in the present problem, we adopt Favre averaging for the density-weighted quantities. We denote the Reynolds-averaged quantity by an overbar, the Favre-averaged quantity by a tilde, and the corresponding fluctuations by a double prime. For example, the velocity is decomposed as $u_i = \tilde{U}_i + u_i''$, where $\tilde{U}_i = \overline{\rho u_i}/\bar{\rho}$ is the Favre-averaged velocity and u_i'' is the corresponding fluctuation.

Algebraic stress models establish a constitutive relation between the Reynolds stress tensor and the mean-flow quantities, thereby eliminating the need to solve additional transport equations for the Reynolds stresses[6, 7]. Following the standard procedure, we relate the Reynolds stress anisotropy tensor $b_{ij} = \widetilde{u_i''u_j''}/2k - 1/3\delta_{ij}$ to the production term P_{ij}, the mass-flux term M_{ij}, the redistribution term Φ_{ij}, and the dissipation term ε_{ij} as follows:

$$P_{ij} + M_{ij} + \Phi_{ij} - \varepsilon_{ij} = 2\left(b_{ij} + \frac{1}{3}\delta_{ij}\right)(P_k + M_k + \Phi_k - \varepsilon) \tag{1}$$

In equation(1),the production term and mass-flux term are defined as equation(2). Notice that the mass-flux term ignored molicular viscosity stress here, because shock is the dominant mechanism for generating mass flux in the present problem.

$$\begin{aligned} P_{ij} &= -\bar{\rho}\left(\widetilde{u_i''u_k''}\frac{\partial \tilde{U}_j}{\partial x_k} + \widetilde{u_j''u_k''}\frac{\partial \tilde{U}_i}{\partial x_k}\right), \quad P_k = \frac{1}{2}P_{ii} \\ M_{ij} &= -\left(\overline{u_i''}\frac{\partial \bar{P}}{\partial x_j} + \overline{u_j''}\frac{\partial \bar{P}}{\partial x_i}\right), \quad M_k = \frac{1}{2}M_{ii} \end{aligned} \tag{2}$$

The redistribution term is modeled by the form of GSG model[8] with parameter C_4 adjusted.

$$\begin{aligned} \Phi_{ij} - \frac{2}{3}\Phi_k\delta_{ij} =& -2C_1\varepsilon b_{ij} + C_2\rho k\left(S_{ij} - \frac{1}{3}S_{kk}\delta_{ij}\right) \\ &+ C_3\rho k\left(b_{ik}S_{jk} + b_{jk}S_{ik} - \frac{2}{3}b_{mn}S_{mn}\delta_{ij}\right) - C_4\left(M_{ij} - \frac{1}{3}M_{kk}\delta_{ij}\right) \\ C_1 = 1.8, C_2 =& 0.8, C_3 = 1.2, C_4 = 0.6 \end{aligned} \tag{3}$$

The dissipation term is modeled as $\varepsilon_{ij} = \frac{2}{3}\varepsilon\delta_{ij}$, which assumes isotropic dissipation. The production term and the mass-flux term are remained at this stage.

Solving the above equation for the full tensor b_{ij} would generally yield an algebraic stress closure involving a large number of tensor bases constructed from S_{ij}, W_{ij}, and M_{ij}. Retaining only the first-order tensor basis would lead to a formulation similar to that of Ristorcelli and Livescu[9]. In the present problem, however, spherical symmetry reduces the Reynolds stress anisotropy tensor to a single independent component, b_{rr}, and all relevant tensors can be simplified accordingly. We therefore solve the equation directly for b_{rr} without introducing a tensor-basis expansion.

$$b_{rr} = \frac{(C_2 - \frac{4}{3})\overline{\rho}k\left(\frac{2}{3}\frac{\partial U_r}{\partial r} - \frac{2}{3}\frac{U_r}{r}\right) - \frac{4}{3}(1 - C_4)\overline{u_r''}\frac{\partial \overline{P}}{\partial r}}{2g - \overline{\rho}k(C_3 - 2)\left(\frac{4}{3}\frac{\partial U_r}{\partial r} + \frac{2}{3}\frac{U_r}{r}\right)}. \tag{4}$$

In the above expression, the term g is defined as

$$g = P_k + M_k + \Phi_k + (C_1 - 1)\,\varepsilon, \tag{5}$$

Notice that the production term P_k is also a function of the Reynolds stress. Here, we follow the modeling approach of Wallin et al.[10], which expresses the production term as a function of the Reynolds stress either, and solve the resulting equation for the Reynolds stress component $\widetilde{u_r''u_r''}$. Since the Reynolds stress component $\widetilde{u_r''u_r''}$ is non-negative and less than $2k$, the final expression is further limited to ensure realizability. The final algebraic stress closure is given by:

$$\begin{aligned}
&\widetilde{u_r''u_r''} = min(2k, \sigma_{rr}), \quad \sigma_{rr} = \frac{|-B + \sqrt{\Delta_2}|}{2|A|} \\
&\Delta_2 = \frac{1}{2}\left(\Delta + sign(\Delta)\Delta\right) \geqslant 0, \quad \Delta = B^2 - 4AC \\
&A = -\bar{\rho}\,(3S_{rr} - S_{kk}) \\
&B = 2M_k + 2\Phi_k + 2(C_1 - 1)\rho\varepsilon + (6 - C_3)\bar{\rho}kS_{rr} - (2 + \frac{1}{3}C_3)\bar{\rho}kS_{kk} \\
&C = \left(-2C_2 + \frac{2}{3}C_3\right)\bar{\rho}k^2S_{rr} + \left(\frac{2}{3}C_2 + \frac{2}{9}C_3\right)\bar{\rho}k^2S_{kk} \\
&\quad - (4 - \frac{8}{3}C_4)kM_k - \frac{4}{3}k\Phi_k - \frac{4}{3}(C_1 - 1)k\rho\varepsilon
\end{aligned} \tag{6}$$

This expression shows that the mass-flux term M_k is directly coupled with Reynolds stress anisotropy, a notable characteristic of the proposed closure.

We evaluate the performance of the proposed algebraic stress closure using a high-fidelity dataset[11] derived from Implicit Large Eddy Simulations (ILES) of a spherically converging Richtmyer-Meshkov instability. The simulations correspond to a Mach number of approximately 1.5 in an SF_6/N_2 mixing with an Atwood number of 0.678.

The results are shown in Figure 1. The proposed algebraic stress closure agrees well with the reference Reynolds stress data at different times, indicating that it captures the Reynolds stress anisotropy in the turbulent mixing process driven by converging spherical shocks.

3. Computational Implementation

To put the proposed algebraic stress closure into practical use, we develop a spherically symmetric RANS code TMS1D(Turbulent Mixing Solver in 1D Spherical Coordinates) to simulate turbulent mixing driven by converging spherical shock waves. This section provides an overview of the governing equations, numerical methods, and turbulence model implemented in the code.

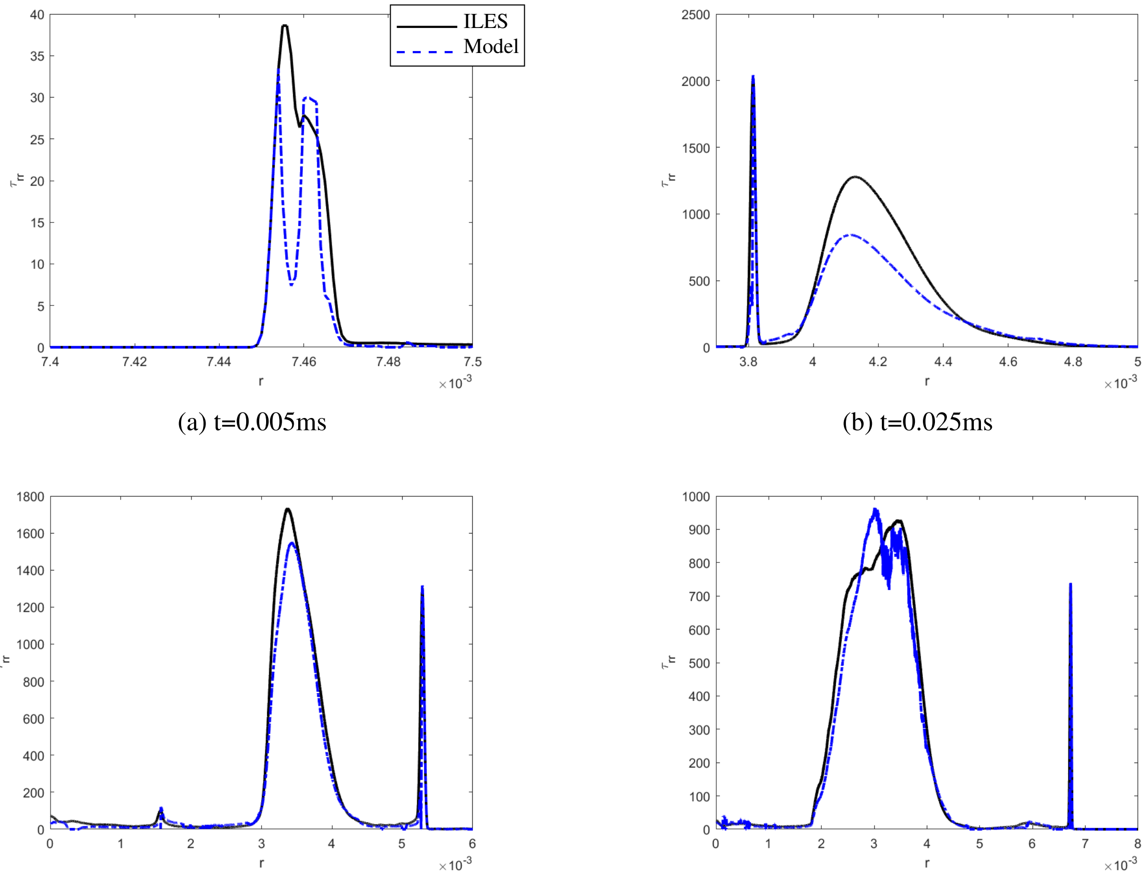

(a) t=0.005ms

(b) t=0.025ms

(c) t=0.035ms

(d) t=0.05ms

Figure 1: Assessment of the proposed algebraic stress closure against reference Reynolds stress data in a spherically converging shock-driven mixing case. The model predictions (blue dashed line) are compared with the reference data (black solid line) at different times. At t = 0.005 ms, the shock wave has just interacted with the perturbed interface. At t = 0.025 ms, the reflected shock wave is about to impinge on the interface again. At t = 0.035 ms, the reflected shock wave has passed through the interface. At t = 0.05 ms, the reflected shock has passed and the mixing layer is in the growth stage.

3.1 Governing equations and numerical methods

The governing equations solved in the present code include the conservation equations for mass, momentum, total energy, and species transport. Under Favre, or density-weighted, averaging, the spherically symmetric RANS equations in the high-Reynolds-number limit, where molecular viscosity, heat conduction, and species diffusion are neglected, are written as

$$\frac{\partial\bar{\rho}}{\partial t}+\frac{1}{r^2}\frac{\partial}{\partial r}\left(r^2\bar{\rho}\tilde{U}_r\right)=0 \tag{7}$$

$$\frac{\partial\bar{\rho}\tilde{U}_r}{\partial t}+\frac{1}{r^2}\frac{\partial}{\partial r}\left[r^2\left(\bar{\rho}\tilde{U}_r^2+\bar{P}\right)\right]=\frac{1}{r^2}\frac{\partial}{\partial r}\left(r^2\tau_{rr}\right)-\frac{\tau_{\theta\theta}+\tau_{\psi\psi}}{r}+\frac{2\bar{P}}{r} \tag{8}$$

$$\frac{\partial\bar{\rho}\tilde{E}}{\partial t}+\frac{1}{r^2}\frac{\partial}{\partial r}\left[r^2\tilde{U}_r\left(\bar{\rho}\tilde{E}+\bar{P}\right)\right]=\frac{1}{r^2}\frac{\partial}{\partial r}\left[r^2\left(\tilde{U}_r\tau_{rr}-q_r\right)\right] \tag{9}$$

$$\frac{\partial\bar{\rho}\tilde{Y}}{\partial t}+\frac{1}{r^2}\frac{\partial}{\partial r}\left(r^2\bar{\rho}\tilde{U}_r\tilde{Y}\right)=-\frac{1}{r^2}\frac{\partial}{\partial r}\left(r^2J_r\right) \tag{10}$$

Here, $\tau_{ij}=-\bar{\rho}\widetilde{u_i''u_j''}$ is the Reynolds stress, q_r is the turbulent heat flux, and J_r is the species diffusion flux. These three terms require closure, and their modeling is specified by the turbulence model introduced below.

For multi-material mixing, the thermodynamic state of the mixture is evaluated using the approach of Kokkinakis et al.[12]:

$$\begin{aligned}\bar{P}&=\bar{\rho}R_*\tilde{T},\\ \gamma&=1+\frac{1}{\sum_{n=1}^{N}\frac{f_n}{\gamma_n-1}},\\ f_n&=\frac{Y_n/M_n}{\sum_{m=1}^{N}Y_m/M_m},\end{aligned} \tag{11}$$

where R_* is the mixture gas constant, f_n is the mole fraction of species n, Y_n is the corresponding mass fraction, M_n is the molecular weight, and γ_n is the ratio of specific heats.

Spatial discretization is performed using the finite volume method (FVM). In spherical coordinates, the governing equations can be written in the following semi-discrete form:

$$\frac{\partial\boldsymbol{U}}{\partial t}+\frac{1}{r^2}\frac{\partial r^2(\boldsymbol{F}-\boldsymbol{F}_v)}{\partial r}=\boldsymbol{S}. \tag{12}$$

Integrating over a spherical-shell control volume gives

$$\int_{r_{i-\frac{1}{2}}}^{r_{i+\frac{1}{2}}}\left[\frac{\partial\boldsymbol{U}}{\partial t}+\frac{1}{r^2}\frac{\partial}{\partial r}\left(r^2\boldsymbol{F}\right)-\frac{1}{r^2}\frac{\partial}{\partial r}\left(r^2\boldsymbol{F}_v\right)\right]4\pi r^2dr=\int_{r_{i-\frac{1}{2}}}^{r_{i+\frac{1}{2}}}\boldsymbol{S}4\pi r^2dr \tag{13}$$

After averaging over the spherical shell, the semi-discrete equation becomes

$$Vol\,\frac{\partial\overline{\boldsymbol{U}}}{\partial t}+A_{i+\frac{1}{2}}F_{i+\frac{1}{2}}-A_{i-\frac{1}{2}}F_{i-\frac{1}{2}}=A_{i+\frac{1}{2}}F_{v,i+\frac{1}{2}}-A_{i-\frac{1}{2}}F_{v,i-\frac{1}{2}}+\int_{r_{i-\frac{1}{2}}}^{r_{i+\frac{1}{2}}}\boldsymbol{S}4\pi r^2dr, \tag{14}$$

where $Vol=\frac{4}{3}\pi(r_{i+1/2}^3-r_{i-1/2}^3)$ and $A_{i\pm1/2}=4\pi r_{i\pm1/2}^2$. Geometrical effects are introduced through the area-weighted fluxes, while the numerical treatment of interfacial fluxes is otherwise identical to that used in Cartesian coordinates.

The numerical schemes are summarized as follows. Convective fluxes are computed using the HLLC approximate Riemann solver[13] together with reconstruction methods of different orders, including zeroth-order reconstruction, minmod reconstruction, and MLP5 reconstruction[14]. Viscous terms are discretized using a second-order central difference scheme, and source terms are integrated explicitly. Time advancement is performed using an explicit third-order TVD Runge–Kutta method. A symmetry boundary condition is imposed at the spherical center, while either a fixed or non-reflecting boundary condition can be applied at the outer boundary.

3.2 Baseline BHR2 model

The baseline model is a parameter-adjusted BHR2 model[15]. In the spherically symmetric case, the BHR2 model can be simplified as follows.

Reynolds stress closure:

$$\begin{aligned}
&\bar{\tau}_{ij} = 2\mu_t \left(S_{ij} - \frac{1}{3}S_{kk}\delta_{ij}\right) - \frac{2}{3}\bar{\rho}k\delta_{ij}, \\
&\mu_t = C_\mu \bar{\rho} l \sqrt{2k}.
\end{aligned} \tag{15}$$

In one-dimensional spherical symmetry, the components are

$$\begin{aligned}
\tau_{rr} &= \frac{4}{3}\mu_t \frac{\partial \tilde{U}_r}{\partial r} - \frac{4}{3}\mu_t \frac{\tilde{U}_r}{r} - \frac{2}{3}\bar{\rho}k, \\
\tau_{\theta\theta} = \tau_{\psi\psi} &= -\frac{2}{3}\mu_t \frac{\partial \tilde{U}_r}{\partial r} + \frac{2}{3}\mu_t \frac{\tilde{U}_r}{r} - \frac{2}{3}\bar{\rho}k.
\end{aligned} \tag{16}$$

Turbulent heat flux and species diffusion:

$$q_r = -\frac{\mu_t}{N_k}\frac{\partial k}{\partial r} - \frac{\mu_t}{N_h}\frac{\partial \tilde{h}}{\partial r}, \quad J_r = -\frac{\mu_t}{N_Y}\frac{\partial \tilde{Y}}{\partial r}, \tag{17}$$

where $\tilde{h} = \tilde{e} + \bar{P}/\bar{\rho}$.

Turbulent kinetic energy transport equation:

$$\begin{aligned}
\frac{\partial \bar{\rho}k}{\partial t} + \frac{1}{r^2}\frac{\partial r^2 \bar{\rho}\tilde{U}_r k}{\partial r} =& \frac{1}{r^2}\frac{\partial}{\partial r}\left(r^2 \frac{\mu_t}{N_k}\frac{\partial k}{\partial r}\right) \\
&+ a_r \frac{\partial \bar{P}}{\partial r} + \left(\tau_{rr}\frac{\partial \tilde{U}_r}{\partial r} + \tau_{\theta\theta}\frac{\tilde{U}_r}{r} + \tau_{\psi\psi}\frac{\tilde{U}_r}{r}\right) - \bar{\rho}\frac{k^{\frac{3}{2}}}{l}.
\end{aligned} \tag{18}$$

Eddy-length-scale transport equation:

$$\begin{aligned}
\frac{\partial \bar{\rho}l}{\partial t} + \frac{1}{r^2}\frac{\partial r^2 \bar{\rho}\tilde{U}_r l}{\partial r} =& \frac{1}{r^2}\frac{\partial}{\partial r}\left(r^2 \frac{\mu_t}{N_l}\frac{\partial l}{\partial r}\right) \\
&+ \frac{l}{k}\left[(\frac{3}{2} - C_4)a_r \frac{\partial \bar{P}}{\partial r} + (\frac{3}{2} - C_1)\left(\tau_{rr}\frac{\partial \tilde{U}_r}{\partial r} + \tau_{\theta\theta}\frac{\tilde{U}_r}{r} + \tau_{\psi\psi}\frac{\tilde{U}_r}{r}\right)\right] \\
&- (\frac{3}{2} - C_2)\bar{\rho}k^{\frac{1}{2}}.
\end{aligned} \tag{19}$$

Mass-flux transport equation for $a_r \equiv -\overline{u_r''}$:

$$\begin{aligned}\frac{\partial \bar{\rho} a_r}{\partial t} + \frac{1}{r^2}\frac{\partial r^2 \bar{\rho} a_r \tilde{U}_r}{\partial r} =& \frac{1}{r^2}\frac{\partial}{\partial r}\left(r^2 \frac{\mu_t}{N_a}\frac{\partial a_r}{\partial r}\right) \\ &+ b\frac{\partial \bar{P}}{\partial r} + \bar{\rho}\left(\frac{\partial a_r^2}{\partial r} + \frac{2a_r^2}{r}\right) - \bar{\rho} a_r \frac{\partial}{\partial r}\left(\tilde{U}_r - a_r\right) \\ &+ \frac{\tau_{rr}}{\bar{\rho}}\frac{\partial \bar{\rho}}{\partial r} - C_a \bar{\rho} a_r \frac{k^{\frac{1}{2}}}{l} - \frac{2}{r^2}\frac{\mu_t}{N_a} a_r.\end{aligned} \tag{20}$$

Density self-correlation transport equation for $b \equiv \overline{\rho'^2}/\bar{\rho}$:

$$\begin{aligned}\frac{\partial \bar{\rho} b}{\partial t} + \frac{1}{r^2}\frac{\partial r^2 \bar{\rho} b \tilde{U}_r}{\partial r} =& \frac{1}{r^2}\frac{\partial}{\partial r}\left(r^2 \frac{\mu_t}{N_b}\frac{\partial b}{\partial r}\right) \\ &+ 2\bar{\rho} a_r \frac{\partial b}{\partial r} - 2(b+1) a_r \frac{\partial \bar{\rho}}{\partial r} \\ &- \frac{2}{\rho}\frac{\mu_t}{N_b}\frac{\partial b}{\partial r}\frac{\partial \rho}{\partial r} - C_b \bar{\rho} b \frac{k^{\frac{1}{2}}}{l}.\end{aligned} \tag{21}$$

The model coefficients are listed in Table 1.

Table 1: BHR2 model coefficients

C_1	C_2	C_4	C_a	C_b	C_μ	N_k	N_l	N_Y	N_h	N_a	N_b
1.50	1.955	1.50	1.13	0.7	2.718	1.503	0.212	0.840	0.840	1.212	0.755

3.3 Algebraic Stress Model

The proposed algebraic stress closure provides a constitutive relation for the Reynolds stress tensor and can be embedded into any turbulence models that solve for the turbulent kinetic energy and turbulent scale. In the present work, it is incorporated into a $k - l$ model modified from the BHR2 model[15]. An algebraic closure is adopted for the mass-flux term, thereby avoiding the need to solve the mass-flux and density self-correlation transport equations in the original BHR2 formulation. The remaining unclosed terms in the algebraic stress closure are modeled following our previous work[16].

In one-dimensional spherical symmetry, the Reynolds stress constitutive relation is written as equation(22), where the radial component $\bar{\tau}_{rr}$ is given by the algebraic stress closure as equation(6), and the other two components are determined by the spherical symmetry and the turbulent kinetic energy k.

$$\begin{aligned}&\bar{\tau}_{rr} = -\bar{\rho}\widetilde{u_r'' u_r''}, \quad \bar{\tau}_{\theta\theta} = -\bar{\rho}\widetilde{u_\theta'' u_\theta''}, \quad \bar{\tau}_{\psi\psi} = -\bar{\rho}\widetilde{u_\psi'' u_\psi''} \\ &\bar{\tau}_{rr} = -\bar{\rho}\min(2k, \max(0, \sigma_{rr})), \quad \bar{\tau}_{\theta\theta} = \bar{\tau}_{\psi\psi} = -\frac{1}{2}(2\bar{\rho}k + \bar{\tau}_{rr})\end{aligned} \tag{22}$$

The terms appearing in the algebraic stress closure are modeled as follows:

$$\begin{aligned}
M_k &= -\overline{u_i''}\frac{\partial \overline{P}}{\partial x_i} = -\frac{\nu_t}{N_\rho \bar{\rho}}\frac{\partial \bar{\rho}}{\partial r}\frac{\partial \bar{P}}{\partial r} \\
\Phi_k &= \overline{p'\frac{\partial u_i'}{\partial x_i}} = -\frac{\partial}{\partial r}\left(C_{k,0}\nu_t M_t\right)\frac{\partial \bar{P}}{\partial r} - C_{k,0}\nu_t M_t \frac{\partial^2 \overline{P}}{\partial r^2} + C_{pd}\nu_t M_t \frac{\partial^2 \bar{P}}{\partial r^2} \\
&- \left(C_{k,0} - C_{pd}\right)\frac{2}{r}\nu_t M_t \frac{\partial \bar{P}}{\partial r} \\
M_t &= \frac{\sqrt{2k}}{c}, \quad c = \sqrt{\gamma R T} = \sqrt{\gamma \bar{P}/\bar{\rho}} \\
S_{rr} &= \frac{\partial \tilde{U}_r}{\partial r}, \quad S_{\theta\theta} = S_{\psi\psi} = \frac{\tilde{U}_r}{r}, \quad S_{kk} = S_{rr} + S_{\theta\theta} + S_{\psi\psi} = \frac{\partial \tilde{U}_r}{\partial r} + \frac{2\tilde{U}_r}{r} \\
\mu_t &= C_\mu \bar{\rho}\tilde{l}\sqrt{2\tilde{k}}, \quad \nu_t = \frac{\mu_t}{\bar{\rho}}, \quad \varepsilon = C_D k^{\frac{3}{2}}/l
\end{aligned} \tag{23}$$

The turbulent kinetic energy equation is

$$\begin{aligned}
\frac{\partial \bar{\rho} k}{\partial t} + \frac{1}{r^2}\frac{\partial (r^2 \rho \tilde{U}_r k)}{\partial r} =& \frac{1}{r^2}\frac{\partial}{\partial r}\left[r^2\left(\frac{\mu_t}{N_k}\frac{\partial k}{\partial r} - C_{k0}\frac{\mu_t}{\rho}M_t\frac{\partial \bar{P}}{\partial r}\right)\right] \\
&+ a_r \frac{\partial \bar{P}}{\partial r} + \left(\tau_{rr}\frac{\partial \tilde{U}_r}{\partial r} + \tau_{\theta\theta}\frac{\tilde{U}_r}{r} + \tau_{\psi\psi}\frac{\tilde{U}_r}{r}\right) - \bar{\rho}\frac{k^{\frac{3}{2}}}{l}
\end{aligned} \tag{24}$$

The eddy-length-scale equation is

$$\begin{aligned}
\frac{\partial \bar{\rho} l}{\partial t} + \frac{1}{r^2}\frac{\partial r^2 \bar{\rho}\tilde{U}_r l}{\partial r} =& \frac{1}{r^2}\frac{\partial}{\partial r}\left(r^2 \frac{\mu_t}{N_l}\frac{\partial \tilde{l}}{\partial r}\right) \\
&+ \frac{l}{k}\left[(\frac{3}{2} - C_{l,4})a_r\frac{\partial \bar{P}}{\partial r} + (\frac{3}{2} - C_{l,1})\left(\tau_{rr}\frac{\partial \tilde{U}_r}{\partial r} + \tau_{\theta\theta}\frac{\tilde{U}_r}{r} + \tau_{\psi\psi}\frac{\tilde{U}_r}{r}\right)\right] \\
&- (\frac{3}{2} - C_{l,2})\bar{\rho}k^{\frac{1}{2}}
\end{aligned} \tag{25}$$

In the transport equations, the mass-flux term is modeled as

$$a_r = -\overline{u_r''} = \frac{\overline{\rho' u_r'}}{\overline{\rho}} = -\frac{\nu_t}{N_\rho \overline{\rho}}\left(\frac{\partial \bar{\rho}}{\partial r} - \frac{\bar{\rho}}{\bar{P}}\frac{\partial \bar{P}}{\partial r}\right) \tag{26}$$

The parameters appearing in the above equations are defined as follows:

Table 2: $ASM - k - l$ model coefficients

C_μ	$C_{k,0}$	C_{pd}	C_1	C_2	C_3	C_4	C_D	$C_{l,1}$	$C_{l,2}$	$C_{l,4}$
2.718	0.3	0.36	1.8	0.8	1.2	0.6	1.0	1.50	1.955	1.50

N_h	N_k	N_Y	N_ρ	N_l
0.840	1.503	0.84	1.0	0.212

4. Spherical Converging Shock-Driven Mixing

Turbulent mixing at a material interface driven by a spherically converging shock is an important theoretical benchmark because it can be regarded as a simplified representation of inertial-confinement-fusion implosion dynamics. This problem has been investigated using ILES by Youngs and Williams[17] and by El Rafei et al[18, 19].

Figure 2 shows a schematic of the physical model. The process can be summarized as follows: a high-pressure source region drives an inwardly converging shock, which reflects between the spherical center and the material interface. The interaction between the shock and the interface then generates turbulent mixing.

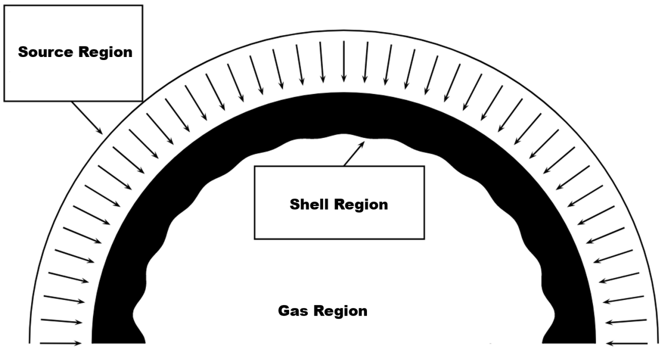

Figure 2: Schematic of material-interface turbulent mixing driven by a spherically converging shock, redrawn from Ref. [20].

The RANS equations are solved in spherical coordinates over the domain $[0, 15]$ cm. The region 0 cm $< r <$ 10 cm is occupied by the gas, with density $\rho_{gas} = 0.05$ g/cm^3, pressure $p_{gas} = 0.1$ g/(cm $\cdot$ s^2), and velocity $u_{gas} = 0$. The region 10 cm $< r <$ 12 cm corresponds to the shell, with density $\rho_{shell} = 1.0$ g/cm^3, pressure $p_{shell} = 0.1$ g/(cm $\cdot$ s^2), and velocity $u_{shell} = 0$.

Both materials are modeled as ideal gases with the same ratio of specific heats, $\gamma = 5/3$. A molecular-weight ratio of 1:20 is prescribed so that the gas and shell regions have the same initial temperature; specifically, $M_{gas} = 0.0288$ kg/mol and $M_{shell} = 0.576$ kg/mol.

The converging shock is driven by a high-pressure source region initially located in 12 cm $< r <$ 15 cm. The inner boundary of the source region moves inward from $r = 12$ cm, and its position is given by

$$r_{src}(t) = 12 - v_0 t \tag{27}$$

where $v_0 = 2.4$ cm/s. The velocity within the source region is prescribed as

$$u_{src}(r,t) = -v_0 \frac{r}{r_{src}(t)} \tag{28}$$

The density in the source region is kept fixed at $\rho_{source} = 0.1$ g/cm^3 throughout the simulation, while the pressure is prescribed as

$$p(t) = \begin{cases} 10 & 0 \le t < 0.5s \\ 10 - 9.9/2.5(t - 0.5) & 0.5s \le t \end{cases} \quad g/(cms^2) \tag{29}$$

The initial state is summarized in Table 3.

The case is computed using TMS1D and validated against the ILES data.

Table 3: Initial state for the material-interface turbulent mixing case driven by a spherically converging shock

Region (cm)	ρ (g/cm^3)	p [g/(cm·s^2)]	M (kg/mol)	u (cm/s)
Gas [$\frac{\Delta r}{2}$, 10]	0.05	0.1	0.0288	0
Shell [10, 12]	1.0	0.1	0.576	0
Source [12, 15 + $\frac{\Delta r}{2}$]	0.1	10	0.576	$v_{src}(r,t)$

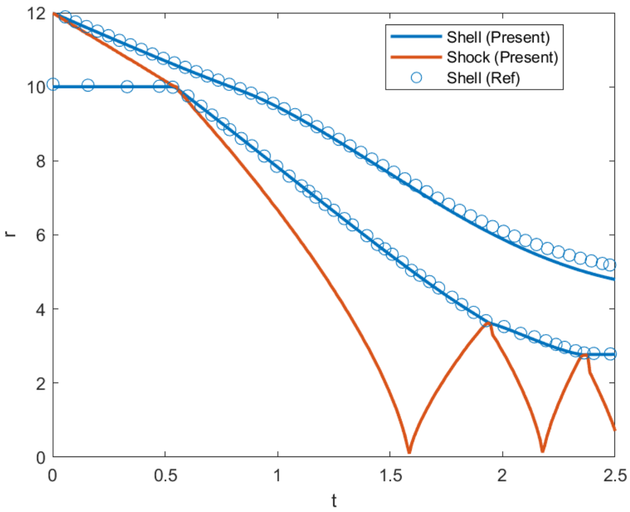

Figure 3: Temporal evolution of the shell and shock positions obtained from the Euler-equation calculation. The reference data are taken from Ref. [17].

First, the computation is performed with the turbulence model turned off. Figure 3 shows the temporal evolution of the shell and shock positions. The results agree well with the ILES reference data[17], indicating that the code captures the basic shock-interface interaction.

We then apply the baseline BHR2 model and the proposed algebraic stress closure to the spherically converging shock-driven mixing case. The initial conditions for the turbulence model are set as follows. For BHR2 model, in the perturbed region ($|r-10| < \Delta r$), the initial TKE, turbulent characteristic length, mass flux velocity, and density-self-correlation are set as $k(0) = 0.02(cm/s)^2, l(0) = 0.04cm, a_r(0) = \sqrt{k(0)}/4$, and $b(0) = 1E-8$, in the other regions, they are set to small numbers near zero. For the $ASM-k-l$ model, in the perturbed region ($|r-10| < \Delta r$), the initial TKE and turbulent characteristic length are set as $k(0) = 0.02(cm/s)^2$ and $l(0) = 0.04cm$,in the other regions, they are also set to small numbers near zero. For both models, 1000 grid points are used in the simulation, and CFL number is set to 0.05.

Figure 4 compares the bubble/spike evolution and the volume fraction profiles predicted by the baseline BHR2 model and the modified ASM-k-l model. Both models agree well with the reference data[17] for these integral quantities, indicating that the algebraic stress closure does not degrade the mean-flow predictions of the baseline formulation.

A further comparison of the radial Reynolds stress anisotropy, b_{rr}, near the center of the mixing layer r_c at $t = 2.2$ is presented in Figure 5. The baseline BHR2 model, which relies on a linear eddy-viscosity relation, fails to adequately reproduce the anisotropy profile and even predicts values outside the Reynolds-stress realizability bounds. In contrast, the proposed algebraic stress closure agrees well with the reference data [18] in the central region of the mixing layer, although it slightly underpredicts the width of the turbulent region.

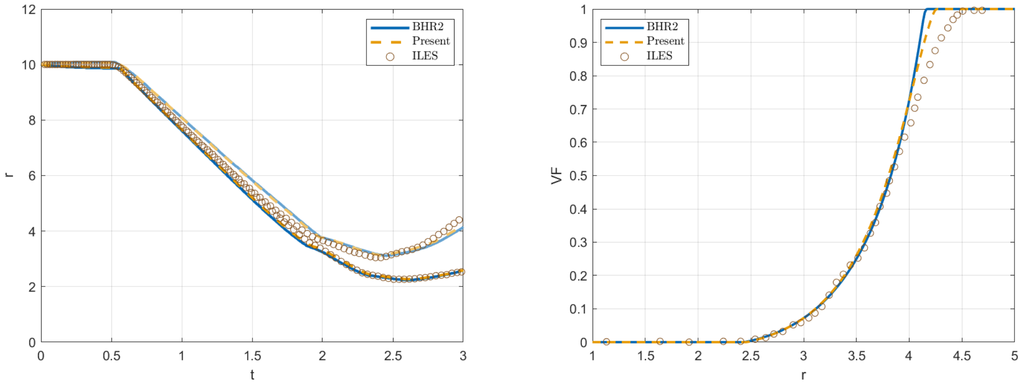

(a) Bubble and spike evolution

(b) Volume fraction distribution at t=3

Figure 4: Simulation results in a spherically converging shock-driven mixing case. ILES reference data are taken from Ref. [17].

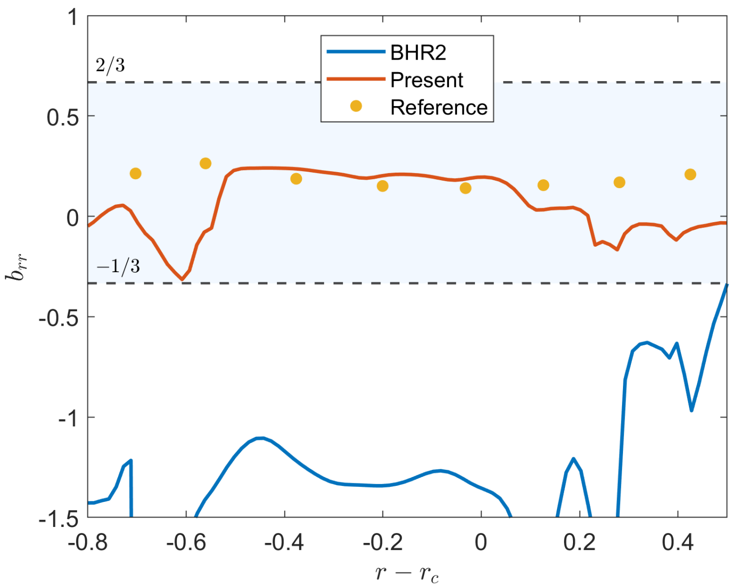

Figure 5: Comparison of Reynolds stress anisotropy b_{rr} between the baseline BHR2 model and the modified $ASM - k - l$ model with the proposed algebraic stress closure, against reference data from Ref. [18] at $t = 2.2$. r_c is the center of the mixing layer, defined as the location where the volume fraction of the shell is 0.5.

These results indicate that the algebraic stress model improves the representation of Reynolds stress anisotropy while maintaining comparable accuracy for the mean-flow quantities. The present case is a preliminary validation problem. Because of its one-dimensional nature, the anisotropic behavior of vector quantities such as heat flux and mass flux remains consistent with a gradient-diffusion approximation. In realistic shock-driven turbulent mixing flows, however, the flow field is expected to be strongly anisotropic, and the directions of heat flux and mass flux may deviate from those predicted by gradient-diffusion models. In such cases, combining the present algebraic stress closure with algebraic closures for vector fluxes is expected to offer further benefits. Further validation in more complex shock-driven turbulent mixing configurations will be pursued in future work.

5. Conclusion and Future Work

In this work, an algebraic stress closure for turbulent mixing driven by converging spherical shocks and a revised $k - l$ model have been developed. The agreement with high-fidelity reference data suggests the potential of the proposed approach for practical CFD applications in compressible variable-density turbulence. Future work will focus on further validation and refinement of the model, especially its extension to more complex shock-driven turbulent mixing scenarios in which spherical symmetry is broken. Additionally, the coupling of the algebraic stress closure with other turbulence models and algebraic closures for vector fluxes will be investigated.

Acknowledgements

This study was funded by the NSFC (Grants 12388101).

References

[1] R. Betti and O. A. Hurricane. Inertial-confinement fusion with lasers. *Nature Physics*, 12(5):435–448, May 2016.
[2] Ye Zhou. Rayleigh–Taylor and Richtmyer–Meshkov instability induced flow, turbulence, and mixing. I. *Physics Reports*, 720–722:1–136, December 2017.
[3] Ye Zhou. Rayleigh–Taylor and Richtmyer–Meshkov instability induced flow, turbulence, and mixing. II. *Physics Reports*, 723–725:1–160, December 2017.
[4] Guy Dimonte and Robert Tipton. K-L turbulence model for the self-similar growth of the Rayleigh-Taylor and Richtmyer-Meshkov instabilities. *Physics of Fluids*, 18(8):085101, August 2006.
[5] Mengjuan Xiao, Yousheng Zhang, and Baolin Tian. Modeling of turbulent mixing with an improved K–L model. *Physics of Fluids*, 32(9):092104, September 2020.
[6] T. B. Gatski and C. G. Speziale. On explicit algebraic stress models for complex turbulent flows. *Journal of Fluid Mechanics*, 254:59–78, September 1993.
[7] S. B. Pope. A more general effective-viscosity hypothesis. *Journal of Fluid Mechanics*, 72(02):331, November 1975.
[8] Olivier Grégoire, Denis Souffland, and Serge Gauthier. A second-order turbulence model for gaseous mixtures induced by Richtmyer—Meshkov instability. *Journal of Turbulence*, 6:N29, January 2005.
[9] J R Ristorcelli and Daniel Livescu. An eddy viscosity expression for Favre averaged Reynolds stresses in vari- able density turbulence. 2006.
[10] Stefan Wallin and Arne V. Johansson. An explicit algebraic Reynolds stress model for incompressible and compressible turbulent flows. *Journal of Fluid Mechanics*, 403:89–132, January 2000.
[11] Xinliang Li, Yaowei Fu, Changping Yu, and Li Li. Statistical characteristics of turbulent mixing in spherical and cylindrical converging Richtmyer–Meshkov instabilities. *Journal of Fluid Mechanics*, 928:A10, December 2021.
[12] Ioannis W. Kokkinakis, Dimitris Drikakis, and David L. Youngs. Modeling of Rayleigh-Taylor mixing using single-fluid models. *Physical Review E*, 99(1):013104, January 2019.

[13] E. F. Toro, M. Spruce, and W. Speares. Restoration of the contact surface in the HLL-Riemann solver. *Shock Waves*, 4(1):25–34, July 1994.

[14] Kyu Hong Kim and Chongam Kim. Accurate, efficient and monotonic numerical methods for multi-dimensional compressible flows: Part II: Multi-dimensional limiting process. *Journal of Computational Physics*, 208(2):570–615, September 2005.

[15] Han-song Xie, Meng-juan Xiao, and You-sheng Zhang. Unified prediction of turbulent mixing induced by interfacial instabilities via Besnard - Harlow - Rauenzahn-2 model. *Physics of Fluids*, 33(10):105123, October 2021.

[16] BoXuan Chen, QiBing Li, XinZhu Li, ShiZhang Huang, WeiRong Wang, and Song Fu. Modeling of turbulent kinetic equation in converging-reflecting spherical shock-turbulence interaction. *SCIENTIA SINICA Physica, Mechanica & Astronomica*, 50(10):104708, October 2020.

[17] David L. Youngs and Robin J. R. Williams. Turbulent mixing in spherical implosions. *International Journal for Numerical Methods in Fluids*, 56(8):1597–1603, 2008.

[18] M. El Rafei, M. Flaig, D. L. Youngs, and B. Thornber. Three-dimensional simulations of turbulent mixing in spherical implosions. *Physics of Fluids*, 31(11):114101, November 2019.

[19] Moutassem El Rafei and Ben Thornber. Turbulence statistics and transport in compressible mixing driven by spherical implosions with narrowband and broadband initial perturbations. *Physical Review Fluids*, 9(3):034501, March 2024.

[20] M. Flaig, D. Clark, C. Weber, D.L. Youngs, and B. Thornber. Single-mode perturbation growth in an idealized spherical implosion. *Journal of Computational Physics*, 371:801–819, October 2018.